Catalysis Today 315 (2018) 205–212

Contents lists available at ScienceDirect

Catalysis Today

journal homepage: www.elsevier.com/locate/cattod

Ag_2MoO_4 nanoparticles encapsulated in g-C_3N_4 for sunlight photodegradation of pollutants

Ming Wu[a,1], Hongying Lv[b,1], Teng Wang[a], Zhimin Ao[a,*], Hongqi Sun[c], Chengyin Wang[b,*], Taicheng An[a], Shaobin Wang[d,*]

[a] Guangzhou Key Laboratory of Environmental Catalysis and Pollution Control, Institute of Environmental Health and Pollution Control, School of Environmental Science and Engineering, Guangdong University of Technology, Guangzhou 51006, China
[b] College of Chemistry and Chemical Engineering, Jiangsu Key Laboratory of Environmental Engineering and Monitoring, Yangzhou University, 180 Si-Wang Ting Road, Yangzhou, 225002, China
[c] School of Engineering, Edith Cowan University, Joondalup, WA 6027, Australia
[d] Department of Chemical Engineering, Curtin University, GPO Box U1987, Perth, WA 6845, Australia

ARTICLE INFO

Keywords:
g-C_3N_4
Ag_2MoO_4
Synergistic effect
Photocatalyst
Pollutant degradation
Sunlight

ABSTRACT

Graphitic carbon nitride (g-C_3N_4), a promising metal-free photocatalyst, shows a high thermal stability, excellent chemical stability, and great optical absorption of solar light. However, a short life of activated electron-hole pairs limits g-C_3N_4 in practical applications. In this work, Ag_2MoO_4 nanoparticles encapsulated in g-C_3N_4 (Ag_2MoO_4/g-C_3N_4) was synthesized with a facile *in-situ* precipitation method. A variety of characterization techniques were applied for analyzing the compositions, morphologies and optical properties of Ag_2MoO_4/g-C_3N_4. The band structure of Ag_2MoO_4 produces a synergistic effect with g-C_3N_4, which can efficiently increase solar light absorption and reduce the recombination rate of the photo-induced electron-hole pairs. Therefore, this hybrid catalyst presents a much higher photocatalytic activity for the degradation of various organic pollutants (bisphenol A, acyclovir, and methyl orange) and strong stability under both artifical and real sunlight, which is promising for practical application.

1. Introduction

Since the 21st century, energy crisis and environmental pollution become more and more serious with the significant growth of population. Water pollution has attracted more attention as resources of drinking water are remarkably reducing. Organic wastes from industries and our daily living are toxic and harmful, which can contaminate water and eventually threaten human health [1]. Some of organic wastes like dyes [2], phenol [3], phenolic compounds [4,5], and pharmaceuticals etc. [6,7] cannot be directly bio-degraded [8,9]. Therefore, treatments of these organic wastes in water have been a hot research topic all over the world. Many methods have been explored, including photocatalysis [8–11], adsorption [12], electrochemical decomposition [13], microbial degradation [14], advanced oxidation [15] and others [16,17]. Photocatalysis is considered as a promising and environmentally friendly method for using clean solar energy and no emission of harmful substances (CO_2 and H_2O). Graphitic carbon nitride (g-C_3N_4) was discovered for water-splitting in 2009, which attracted great attention afterwards from all over the word [18–20]. Meanwhile, the excellent properties of g-C_3N_4, such as great thermal and chemical stability, good optical absorption for sunlight, make it one of the most popular photocatalysts in environmental and energy applications [21–23]. However, pristine g-C_3N_4 has not yet reached the requirements for practical applications due to the short time of the recombination of photogenerated electron-hole pairs [24,25].

Introduction of Ag or its compounds is considered as an effective strategy to enhance the photocatalytic activity of g-C_3N_4 by hindering the electron-hole recombination. For example, Ag [26–28], Ag_2O [29–32], Ag_2CO_3 [33], $Ag_2Mo_2O_7$ [34], Ag_3VO_4 [35], Ag_3PO_4 [36,37], Ag/$AgWO_3$ [38], and Ag/AgBr [39–43] have been attempted for enhancing photocatalytic activity of pristine g-C_3N_4. Another Ag-based compound, Ag_2MoO_4, was also investigated because of its excellent properties like great electrical conductivity, high antimicrobial activity, nontoxicity and great photocatalytic activity [44–48] for degradation of organic dyes. However, it can only be excited under ultraviolet light irradiation due to a wide bandgap of 3.05 eV [49–51]. Recently, Ag_2MoO_4/g-C_3N_4 was reported for degradation of a dye under visible light irradiation [52], but more research on its synthesis, catalytic

* Corresponding authors.
E-mail addresses: zhimin.ao@gdut.edu.cn (Z. Ao), wangcy@yzu.edu.cn (C. Wang), shaobin.wang@curtin.edu.au (S. Wang).
[1] These authors contributed equally to this work.

https://doi.org/10.1016/j.cattod.2018.01.019
Received 13 November 2017; Received in revised form 12 January 2018; Accepted 16 January 2018
Available online 03 February 2018
0920-5861/

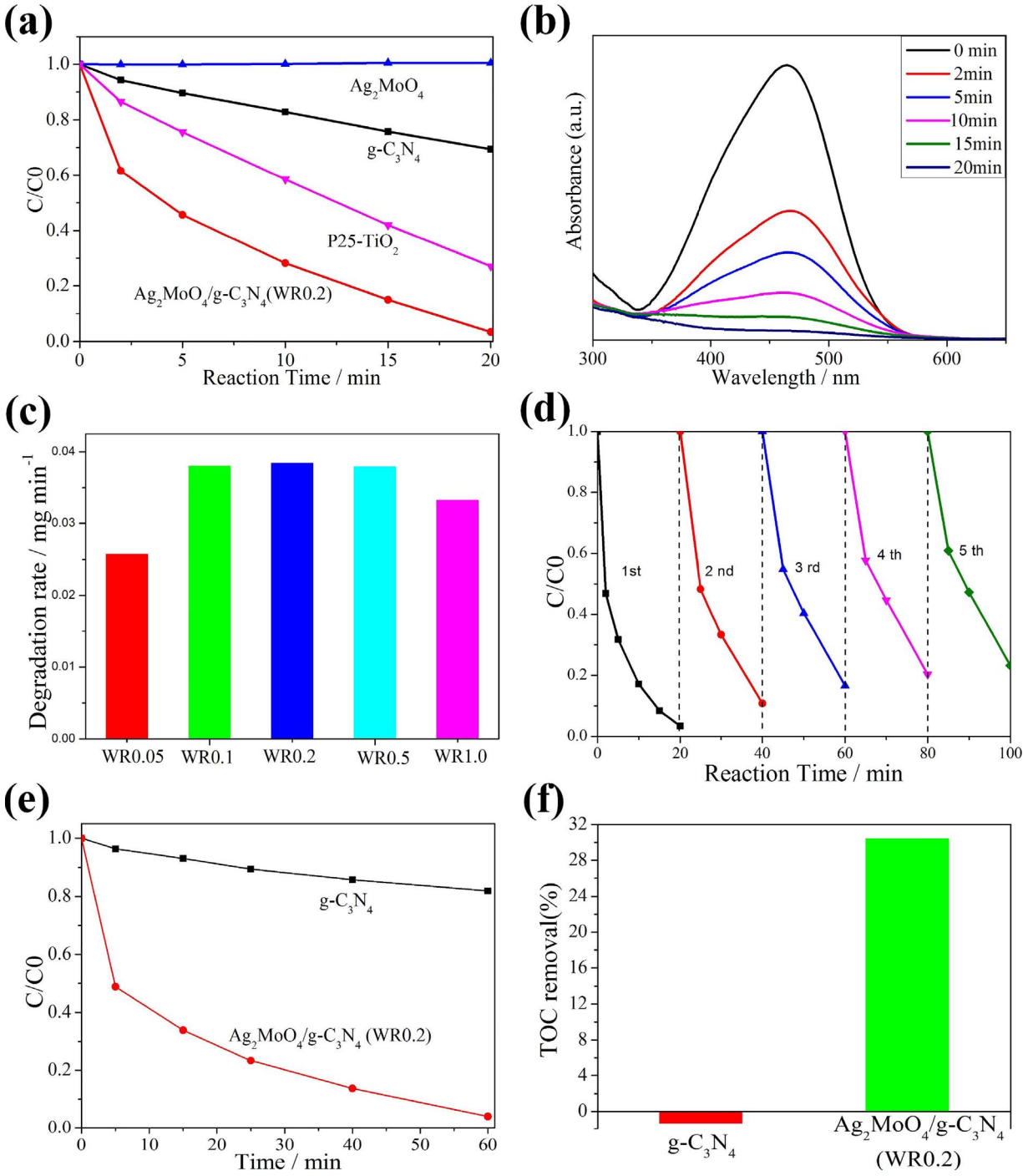

Fig. 1. (a) Photodegradation of MO with Ag_2MoO_4, g-C_3N_4, Ag_2MoO_4/g-C_3N_4(WR0.2) and P25-TiO_2. (b) The given time UV/Vis spectrum of MO degradation solution by Ag_2MoO_4/g-C_3N_4(WR0.2). (c) Photodegradation rate of MO with different Ag_2MoO_4/g-C_3N_4 samples under 20 min reaction. (d) Recycle tests of Ag_2MoO_4/g-C_3N_4(WR0.2) for photodegradation of MO. The photocatalytic reactions of (a-d) were conducted with simulated sunlight (Xe-light). (e) Photodegradation of MO with g-C_3N_4 and Ag_2MoO_4/g-C_3N_4(WR0.2) under natural sunlight irradiation. (f) TOC removal of MO degraded by g-C_3N_4 and $AgMoO_4$/g-C_3N_4 (WR0.2) after photocatalytic reaction under natural sunlight irradiation.

mechanism and wide application for different organic pollutants is still required.

In this paper, we report a simple synthesis of Ag_2MoO_4/g-C_3N_4 hybrids using a facile *in-situ* precipitation method. The Ag_2MoO_4/g-C_3N_4 samples showed much higher photocatalytic activity than pristine g-C_3N_4 in degradation of organic pollutants including bisphenol A, acyclovir, and methyl orange (MO) under sunlight irradiation. The photocatalytic reaction mechanism and enhancement mechanism of this hybrid catalyst under sunlight were also investigated.

2. Experiments

2.1. Chemicals

Urea ($CO(NH_2)_2$, Aladdin Chemistry Reagent Co., Ltd, ≥99.5%), sodium molybdate ($Na_2MoO_4{\cdot}2H_2O$, Tianjin Chemical Reagent Co., Ltd, ≥99.0%), silver nitrate ($AgNO_3$, Guangzhou Jinhua Chemical Reagent Co., Ltd, ≥99.8%) were used with no further purification. Ultrapure water with a resistance of 18.2 MΩ·cm was obtained from an instrument Unique-R20.

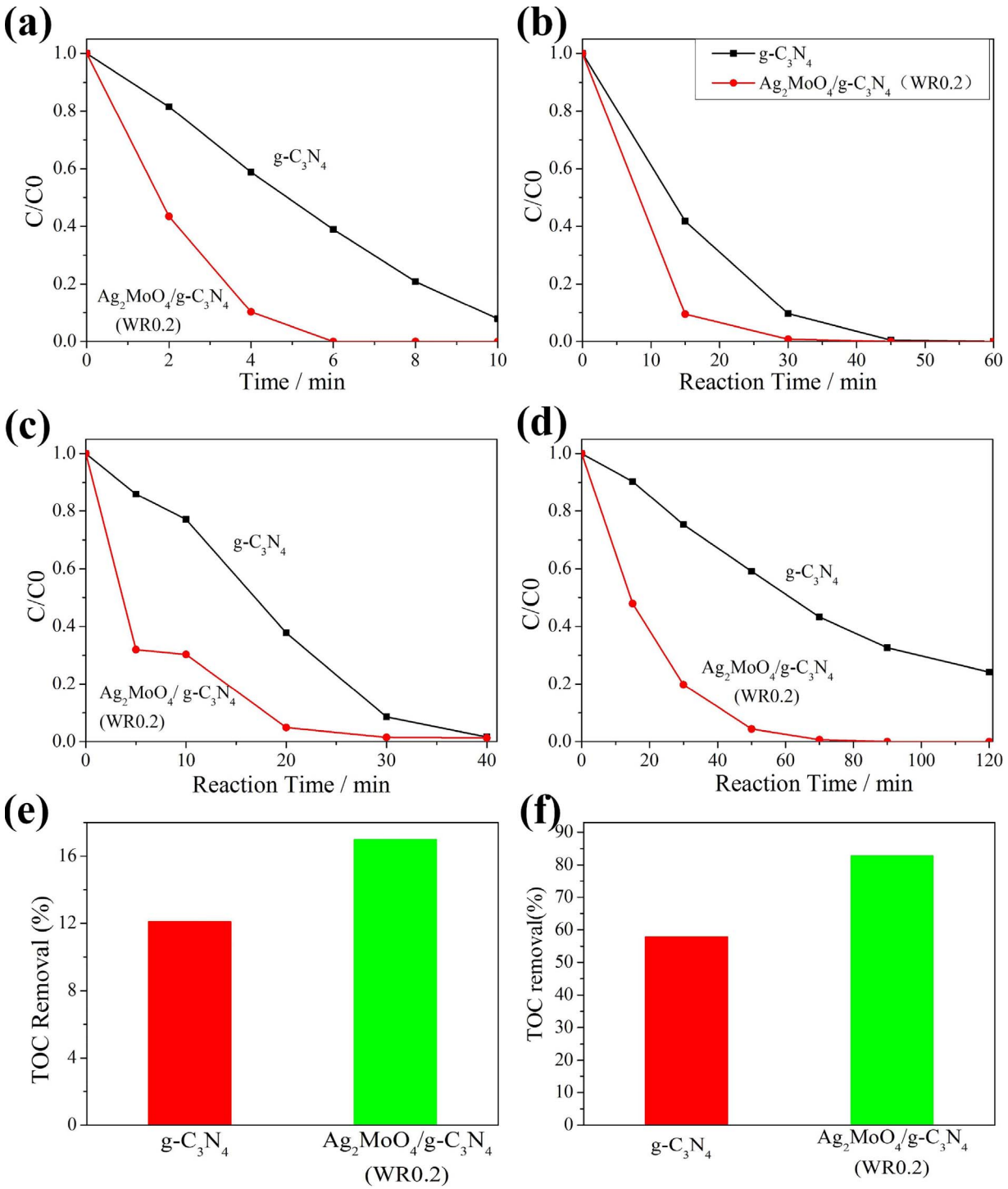

Fig. 2. Photodegradation of acyclovir (a) and bisphenol A (b) with g-C_3N_4 and Ag_2MoO_4/g-C_3N_4(WR0.2) under simulated sunlight irradiation; Photodegradation of acyclovir (c) and bisphenol A (d) with g-C_3N_4 and Ag_2MoO_4/g-C_3N_4(WR0.2) under natural sunlight irradiation (b); TOC removal of acyclovir (e) and bisphenol A (f) degraded by g-C_3N_4 and $AgMoO_4$/g-C_3N_4 (WR0.2) after photocatalytic reaction under natural sunlight irradiation.

2.2. Preparation of samples

g-C_3N_4 powder was synthesized following the method reported by Chen et al. [53]. The urea was placed into an alumina crucible with a cover, and then put into a furnace. The temperature was raised to 550 °C (a ramp rate of 10 °C min^{-1}) and calcined in static air for 4 h. After natural cooling to ambient temperature, g-C_3N_4 sample was collected for Ag_2MoO_4/g-C_3N_4 preparation. Typically, g-C_3N_4 (200 mg) was put into water (50 mL) with 1 h sonication for dispersion. After that, $AgNO_3$ (36.2 mg, 0.21 mmol) was added into the solution with magnetic stirring under room temperature for 1 h. Then, Na_2MoO_4 aqueous solution (5.2 mL, 0.04 M) was put into this solution with another 1 h magnetic stirring. Ag_2MoO_4/g-C_3N_4 at a weight ratio of 0.2 was obtained with water washing for 3 times and dried at 60 °C for 12 h, referring as Ag_2MoO_4/g-C_3N_4 (WR0.2). In addition, other Ag_2MoO_4/g-C_3N_4 samples at weight ratios of WR = 0.05, 0.1, 0.5, 1.0 were synthesized with the similar method, and pure Ag_2MoO_4 was also synthesized without using g-C_3N_4.

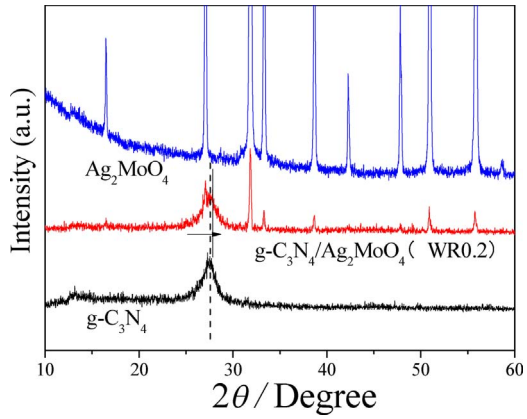

Fig. 3. (a) XRD patterns of Ag_2MoO_4, pristine g-C_3N_4 and Ag_2MoO_4/g-C_3N_4 (WR0.2).

2.3. Photocatalytic test

The photocatalytic reaction was operated with a Xeon lamp (300W, Microsolar 300) under magnetic stirring with 20 mg photocatalyst (0.25 g L^{-1}) in bisphenol A, acyclovir or methyl orange (MO) solution (80 mL, 10 mg L^{-1}). The position of light source was placed 20 cm (the vertical distance) above the reaction solution. Natural sunlight photocatalytic reaction was operated on the roof of the laboratory building (MO: 10:54 to 11:54 AM on May 27, 2017; acyclovir: 09:47 to 10:27 AM on May 27, 2017; bisphenol A: 14:00 to 16:00 PM on June 06, 2017). The amount of catalyst, concentration and volume of organic pollutants are all the same as the photocatalytic reaction under the simulated sunlight. At given reaction time, 3 mL of the mixture reaction solution was collected for determination of pollutant concentration. The best Ag_2MoO_4/g-C_3N_4 sample was applied for the stability tests as follows: after degradation of MO, the sample was collected after water washing for 2 times to achieve a pure sample for the next cycle experiment. To analyze the main active species of Ag_2MoO_4/g-C_3N_4, three different scavengers including *tert*-butyl alcohol (TBA, 10 mM), disodium ethylenediaminetetraacetate (EDTA-2Na, 10 mM) and benzoquinone (BQ, 10 mM) have been used for photodegradation of acyclovir.

2.4. Catalyst characterizations

The structure of the samples can be analyzed with powder X-ray diffraction (XRD), which can be operated on a Rigaku D/max-Ultima IV X-ray diffractometer (a scan rate of 8°/min). A S-4800 II field-emission scanning electron microscope (FESEM) (acceleration voltage of 15 kV) was applied for analyzing the morphology of the samples. The morphology and structures of the samples can be further confirmed with a transmission electron microscope (TEM) of Tecnai G2 F30 S-TWIN. X-ray photoelectron spectroscopy (XPS) data were obtained for the chemical composition of the samples, which was operated on an ESCALAB 250Xi spectrometer with a C1 s reference peak of 284.6 eV. The UV–vis absorption of MO and diffuse reflection spectra of samples were all tested on a spectrophotometer of Agilent Cary 300. A PL-4500 fluorescence spectrophotometer has been used for analyzing the photoluminescence (PL) of the samples. The total organic carbon (TOC) was measured on a TOC-V_{CPH} Total Organic Carbon Analyzer (SHIMADZU). The photoelectrochemical test was operated on an electrochemical workstation (CHI650E) with a standard three-electrode system.

3. Results and discussion

3.1. Photocatalytic activity

Photo-degradation of MO was firstly tested using artificial sunlight. As shown in Fig. 1a, MO cannot be degraded by pure Ag_2MoO_4, while the degradation occurs in the cases of both g-C_3N_4 and Ag_2MoO_4/g-C_3N_4 (WR0.2). MO in the solution can be degraded at 97% by Ag_2MoO_4/g-C_3N_4 (WR0.2) in 20 min while only 30% MO is degraded by the pristine g-C_3N_4 within the same time. In addition, the photocatalytic degradation activity of Ag_2MoO_4/g-C_3N_4 (WR0.2) is better than that of commonly used P25-TiO_2 with degradation efficiency of 73%. The variations of MO absorption spectra during the degradation by Ag_2MoO_4/g-C_3N_4 (WR0.2) are displayed in Fig. 1b, where the peak intensity at 464 nm decreases with the degradation time. Photocatalytic degradation activities of different Ag_2MoO_4/g-C_3N_4 samples are shown in Fig. 1c. With increasing weight ratio of Ag_2MoO_4, Ag_2MoO_4/g-C_3N_4 presents the highest MO degradation efficiency at an optimal ratio of 0.2.

The stability of Ag_2MoO_4/g-C_3N_4 (WR0.2) was also performed (Fig. 1d). During 100 min of 5-cycle photo-degradation reaction, Ag_2MoO_4/g-C_3N_4 (WR0.2) has a stable photo-degradation activity, and after the 4th recycling experiment, about 77% MO solution can still be degraded within 20 min, which is better than that of pristine g-C_3N_4 (only degradation of 30% MO). In addition, photo-degradation of MO under natural sunlight shows (Fig. 1e) 96% MO solution can be degraded by Ag_2MoO_4/g-C_3N_4 (WR0.2) within 60 min, while only 18% MO solution can be degraded by g-C_3N_4 for the same time interval. In addition, Ag_2MoO_4/g-C_3N_4 (WR0.2) also has much better performance than that of the pristine g-C_3N_4 in mineralization of MO under natural sunlight irradiation (Fig. 1f), while the TOC value of g-C_3N_4 is negative, which may be caused by the dissolution of g-C_3N_4 in solution.

Ag_2MoO_4/g-C_3N_4 was also tested for degradation of other pollutants including acyclovir (Fig. 2a, c, and e) and bisphenol A (Fig. 2b, d and f).

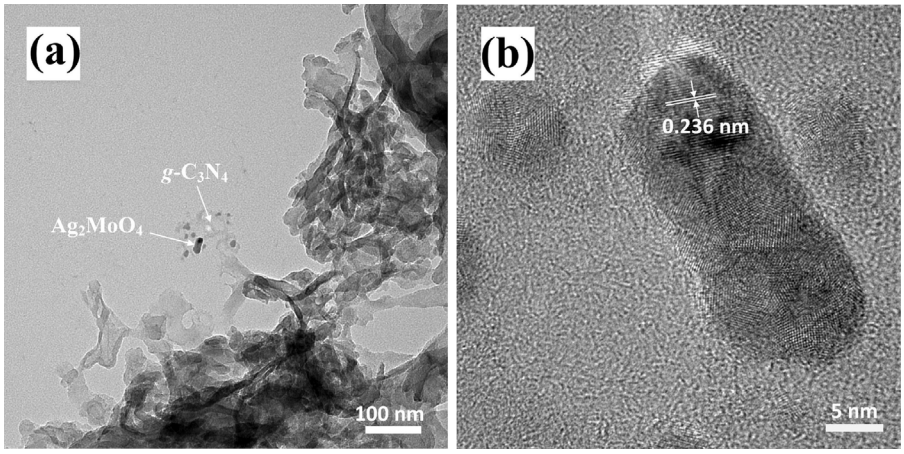

Fig. 4. (a) TEM image and (b) HRTEM image of Ag_2MoO_4/g-C_3N_4(WR0.2).

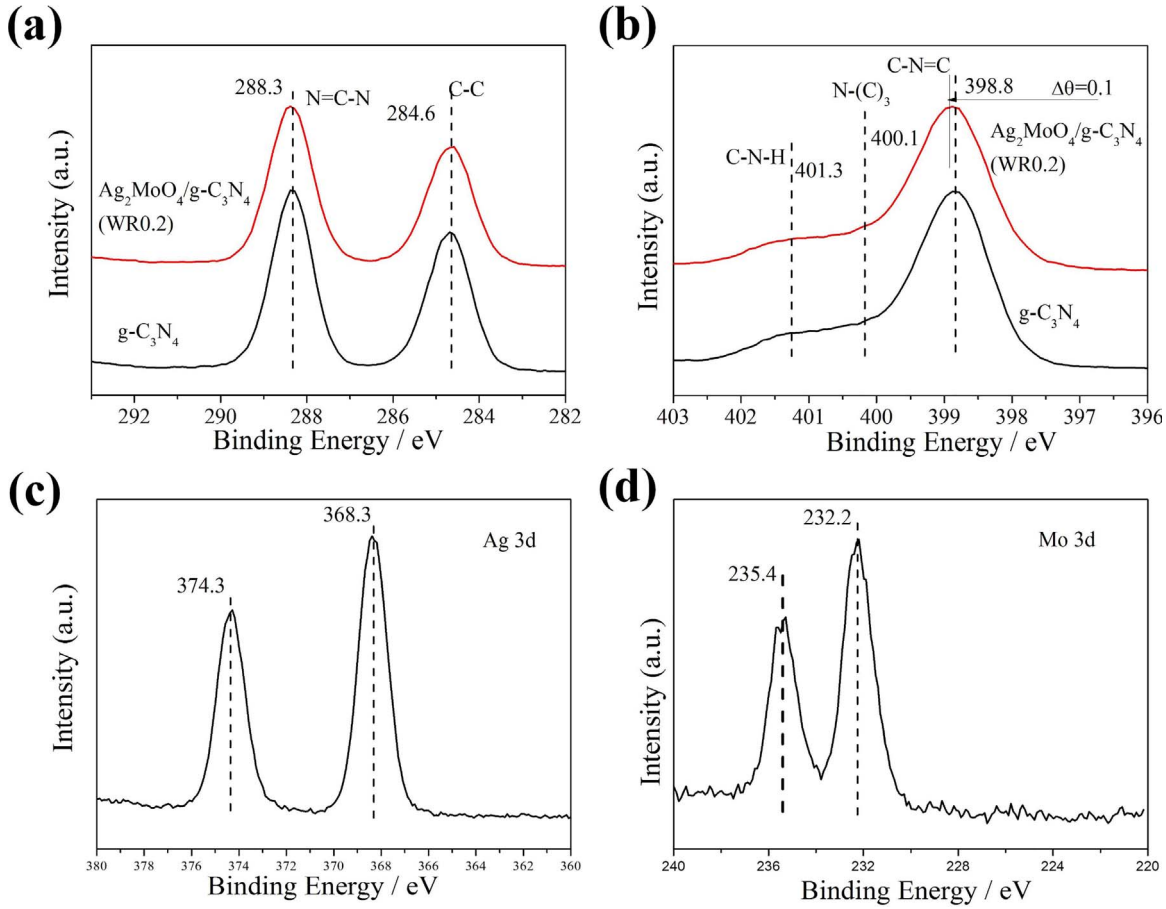

Fig. 5. (a) The C XPS high-resolution and (b) the N XPS high-resolution spectra of the g-C_3N_4 and Ag_2MoO_4/g-C_3N_4(WR0.2), (c) The Ag XPS high-resolutions and (d) the Mo XPS high-resolution spectra of Ag_2MoO_4/g-C_3N_4(WR0.2).

Ag_2MoO_4/g-C_3N_4 (WR0.2) has demonstrated higher photocatalytic degradation efficiencies of acyclovir (Fig. 2a) and bisphenol A (Fig. 2b) than those of pristine g-C_3N_4 under both artificial and natural sunlight (Fig. 2c, d). As shown in Table S1, Ag_2MoO_4/g-C_3N_4 has higher photodegradation activities for degradation of acyclovir and bisphenol A compared with other similar composites based on g-C_3N_4. In addition, the mineralization of the pollutants (acyclovir or bisphenol A) by Ag_2MoO_4/g-C_3N_4 (WR0.2) is better than pristine g-C_3N_4 under natural sunlight irradiation (Fig. 2e and f). Therefore, Ag_2MoO_4/g-C_3N_4 (WR0.2) has significantly enhanced photocatalytic activities as compared to pristine g-C_3N_4, and can also degrade different organic pollutants efficiently into CO_2 and H_2O under natural sunlight irradiation. Moreover, we can find that acyclovir can be most easily degraded by Ag_2MoO_4/g-C_3N_4 (WR0.2) and it can be completely degraded within 6 min. However, among these three pollutants, bisphenol A has the highest mineralization rate ~80% after being degraded completely. Therefore, photocatalytic performance of g-C_3N_4 for serval organic pollutants can be improved significantly with the addition of Ag_2MoO_4, and Ag_2MoO_4/g-C_3N_4 (WR0.2) has the best performance for the degradation of MO.

3.2. Morphology and structure

Crystal structures of Ag_2MoO_4/g-C_3N_4 (WR0.2), pure g-C_3N_4 and Ag_2MoO_4 are shown in Fig. 3. Two main XRD peaks of g-C_3N_4 can be found at 27.5°, related to interlayer reflection [54,55], and 13.2° referring to in-plane structure of g-C_3N_4 [56,57]. The peak at 27.5° of Ag_2MoO_4/g-C_3N_4 (WR0.2) shows a slight shift to a larger 2θ value, which means that the interlayer of g-C_3N_4 is decreased after Ag_2MoO_4 deposition. Meanwhile, the XRD pattern of Ag_2MoO_4/g-C_3N_4 reveals the presence of Ag_2MoO_4 (JCPDS card no. 08-0473). Therefore, Ag_2MoO_4/g-C_3N_4 was successfully synthesized, and Ag_2MoO_4 has strong contact with g-C_3N_4 without structural destruction of g-C_3N_4.

The morphology of the samples was analyzed by SEM (Fig. S1) and TEM (Fig. 4). Ag_2MoO_4/g-C_3N_4(WR0.2) has a similar morphology to the pristine g-C_3N_4 as shown in Fig. S1, which has a bulk structure assembled by small nanosheets. The TEM image of Ag_2MoO_4/g-C_3N_4(WR0.2) suggests that Ag_2MoO_4 nanoparticles are well incorporated with g-C_3N_4, where Ag_2MoO_4 nanoparticles are formed and capsulated by g-C_3N_4 sheets. The size of Ag_2MoO_4 nanoparticles is smaller than 20 nm as indicated in Fig. 4a. HRTEM image of a particle also reveals the crystalline nature of Ag_2MoO_4. Its lattice spacing was confirmed to be 0.236 nm, which is similar to that of (400) plane of Ag_2MoO_4 (JCPDS card no. 08-0473). The presence of Ag_2MoO_4 can also be confirmed with the elemental mapping data (Fig. S2), which also indicates the uniform distribution of C, N, O, Ag and Mo elements in the Ag_2MoO_4/g-C_3N_4 sample. Meanwhile, the specific surface areas of Ag_2MoO_4/g-C_3N_4 (WR0.2) and pristine g-C_3N_4 have been determined as shown in Fig. S3. After Ag_2MoO_4 addition, the specific surface area of Ag_2MoO_4/g-C_3N_4 (70.7 m^2/g) is slightly lower than pristine g-C_3N_4 (96.2 m^2/g), which may be caused by the deposition of capsulated Ag_2MoO_4 in the pores of g-C_3N_4.

3.3. XPS (X-ray photoelectron spectroscopy) analysis

The chemical compositions of Ag_2MoO_4/g-C_3N_4 and pristine g-C_3N_4 were characterized by XPS analysis. The C and N high resolution spectra of g-C_3N_4 and Ag_2MoO_4/g-C_3N_4 are shown in Fig. 5. The C 1s peak of g-C_3N_4 at 284.6 eV is related to C—C bond while the peak of 288.3 eV is related to sp^2-bond carbon (C—C═N) [58,59]. The related

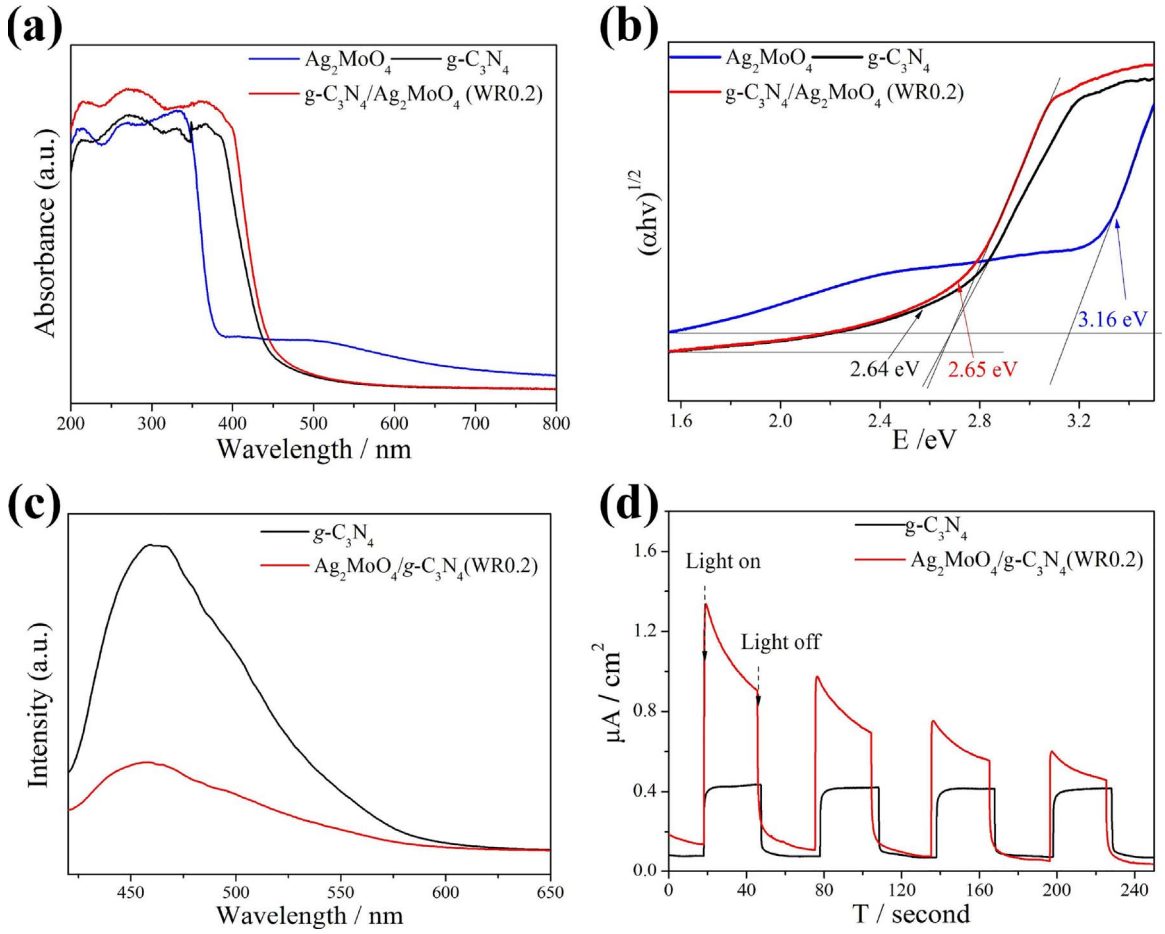

Fig. 6. (a) UV–vis absorption analysis of Ag_2MoO_4, g-C_3N_4 and Ag_2MoO_4/g-C_3N_4 (WR0.2), (b) bandgap of Ag_2MoO_4, g-C_3N_4 and Ag_2MoO_4/g-C_3N_4 (WR0.2), (c) the photoluminescence spectra (PL) of g-C_3N_4 and Ag_2MoO_4/g-C_3N_4 (WR0.2) with the 400 nm excitation, (d) photocurrent test of g-C_3N_4 and Ag_2MoO_4/g-C_3N_4 (WR0.2).

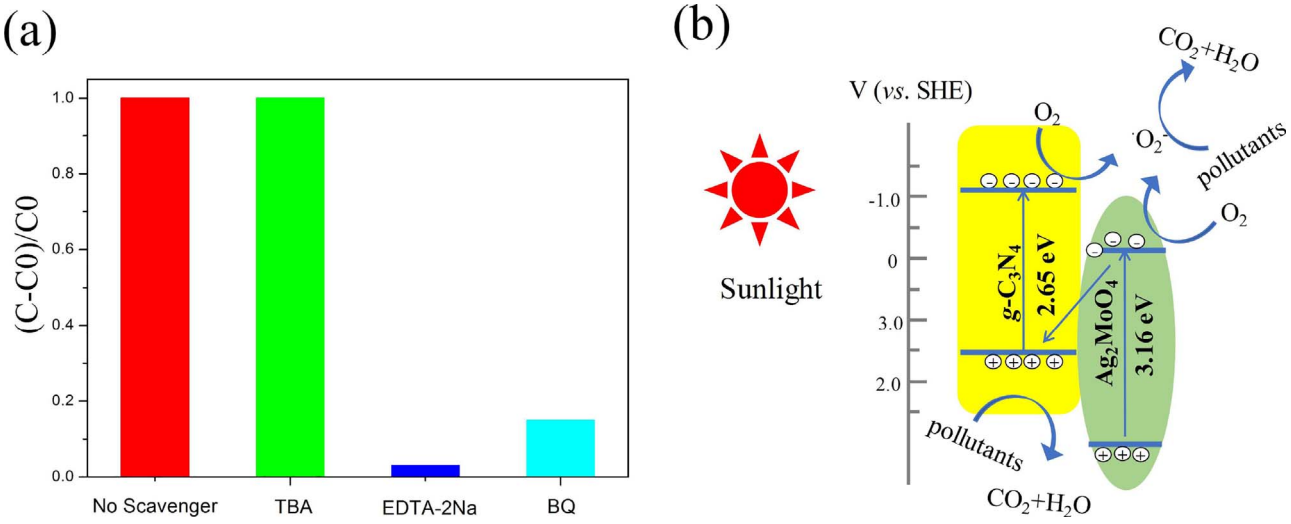

Fig. 7. (a) Degradation rate of Ag_2MoO_4/g-C_3N_4 (WR0.2) with different scavenger adding under simulated sunlight irradiation within 6 min, (b) Photocatalytic degradation mechanism over Ag_2MoO_4/g-C_3N_4 (WR0.2) under sunlight irradiation.

peaks of C 1s in Ag_2MoO_4/g-C_3N_4 did not change. In N 1s spectra of g-C_3N_4 (Fig. 5b), the peak at 398.8 eV is related to the sp^2-hybridized nitrogen in aromatic rings (C—N=C) while the peak at 400.1 eV is regarded as the tertiary nitrogen groups (N—$(C)_3$). The weak peak at 401.3 eV is usually taken as amino functions (C—N—H) [18]. There is a slight peak shift of N 1 s at 398.8 eV for Ag_2MoO_4/g-C_3N_4, which indicates an electron transfer between Ag_2MoO_4 and g-C_3N_4 due to heterojunction between Ag_2MoO_4 and g-C_3N_4. The presence of Ag and Mo elements can also be confirmed by Ag and Mo XPS analysis. As shown in Fig. 5c, two peaks at 368.3 and 374.2 eV are related to the Ag^+ of Ag_2MoO_4 [60], while the two peaks at 232.2 and 235.3 eV are attributed to the Mo^{6+} in Ag_2MoO_4 as shown in Fig. 5d [60].

3.4. Optical analysis

The electronic and optical properties were illustrated in UV–vis diffuse reflectance spectra and photoluminescence spectra (PL). As shown in Fig. 6a, Ag_2MoO_4/g-C_3N_4 has a stronger sunlight absorption region than both Ag_2MoO_4 and g-C_3N_4, which induces enhanced photocatalysis compared to pristine g-C_3N_4. In addition, the bandgap of Ag_2MoO_4/g-C_3N_4 has been determined to 2.65 eV (Fig. 6b), which is almost the same as the bandgap of g-C_3N_4 determined to be 2.64 eV in the figure. However, from PL spectra (Fig. 6c), the emission peak of Ag_2MoO_4/g-C_3N_4 has a much lower intensity, which indicates that the Ag_2MoO_4/g-C_3N_4 has a much lower electron-hole recombination rate compared with that of pristine g-C_3N_4. In addition, the enhanced photogenerated electron-hole pairs of Ag_2MoO_4/g-C_3N_4 were also confirmed by the photocurrent test under artificial sunlight irradiation. From Fig. 6d, a higher photocurrent density can be achieved with Ag_2MoO_4/g-C_3N_4 system than that of g-C_3N_4 under the same conditions. Therefore, the improvement of the photocatalytic activity of Ag_2MoO_4/g-C_3N_4 may be mainly contributed by the heterojunction between Ag_2MoO_4 and g-C_3N_4, which can hinder the recombination rate of photogenerated hole-electron pairs.

3.5. Mechanistic analysis

The photocatalytic activation of Ag_2MoO_4/g-C_3N_4 (WR0.2) was investigated and the active species were detected by a trapping experiment (Fig. 7a) under artificial sunlight irradiation. In the trapping experiment, *tert*-butyl alcohol (TBA) was used for trapping hydroxyl radicals (·OH), disodium ethylenediaminetetraacetate (EDTA-2Na) for detecting holes (h^+) and benzoquinone (BQ) for detecting superoxide radicals (·O_2−) [61,62]. After 6 min photocatalytic reaction of acyclovir under simulated sunlight irradiation, 100% acyclovir can be degraded with TBA addition, while 3.1% and 14.9% acyclovir can be degraded with addition of EDTA-2Na and BQ, respectively. Therefore, hydroxyl radicals (·OH) are not the active species of Ag_2MoO_4/g-C_3N_4 (WR0.2) for acyclovir degradation under simulated sunlight irradiation, while holes (h^+) and superoxide radicals (·O_2−) are the main active species for photo-degradation of the pollutant. Therefore, the mechanism in the enhanced photocatalytic degradation on Ag_2MoO_4/g-C_3N_4 for organic pollutants can be proposed in Fig. 7b. g-C_3N_4 has a higher conduction band (CB, −1.12 eV, *vs.* SHE) compared with that of Ag_2MoO_4 (−0.125 eV, *vs.* SHE), while the valence band (VB) of g-C_3N_4 is lower than that of Ag_2MoO_4 [2,29]. Meanwhile, both g-C_3N_4 and Ag_2MoO_4 can be excited under sunlight irradiation. According to the theory of Z-scheme [63], the photo-generated electrons excited by Ag_2MoO_4 can be recombined with the holes from VB of g-C_3N_4; then photogenerated electrons from the CB of g-C_3N_4 and holes from VB of Ag_2MoO_4 can be increased. Therefore, the photogenerated electrons and holes used for degradation can be increased, and the photocatalytic degradation rate of pollutants on Ag_2MoO_4/g-C_3N_4 can be improved significantly.

4. Conclusions

Ag_2MoO_4/g-C_3N_4 hybrid photocatalysts were successfully obtained by using a facile *in-situ* precipitation method and Ag_2MoO_4/g-C_3N_4 showed much better optical properties and lower recombination of photogenerated electron-hole pairs than pristine g-C_3N_4 for sunlight utilization. Ag_2MoO_4/g-C_3N_4 (WR0.2) demonstrated highly improved photocatalytic degradation performance for different organic pollutants (MO, acyclovir and bisphenol A) under sunlight irradiation, and they can be degraded into CO_2 and H_2O efficiently. Furthermore, based on the trapping experiment, the main active species of photo-degradation of acyclovir catalyzed by Ag_2MoO_4/g-C_3N_4 are holes (h^+) and superoxide radicals (·O_2−). Ag_2MoO_4/g-C_3N_4 also presented strong cycling stability with 77% MO degradation after 5 cycles, demonstrating that it is a promising photocatalyst for the treatment of organic wastes under natural sunlight.

Acknowledgments

This work is financially supported by “1000 plan” for Young Professionals Program of China, “100 Talents” Program of Guangdong University of Technology, National Natural Science Foundation of China (Grant Nos. 21777033, 21607029, 41373102), National Natural Science Funds for Distinguished Young Scholars (41425015), Science and Technology Program of Guangdong Province (2017B020216003), and Science and Technology Program of Guangzhou City (201707010359).

Appendix A. Supplementary data

Supplementary data associated with this article can be found, in the online version, at https://doi.org/10.1016/j.cattod.2018.01.019.

References

[1] Y. Li, P.F. Wang, C.P. Huang, W.F. Yao, Q. Wu, Q.J. Xu, Appl. Catal. B 205 (2017) 489–497.
[2] M. Wu, J.M. Yan, M. Zhao, Q. Jiang, ChemPlusChem 77 (2012) 931–935.
[3] X.G. Duan, Z.M. Ao, H.Q. Sun, ACS Appl. Mater. Interfaces 7 (2015) 4169–4178.
[4] C.F. Mu, Y. Zhang, W.Q. Cui, Y.H. Liang, Y.F. Zhu, Appl. Catal. B 212 (2017) 41–49.
[5] Y.B. Wang, X. Zhao, D. Cao, Y. Wang, Y.F. Zhu, Appl. Catal. B 211 (2017) 79–88.
[6] G.Y. Li, X. Nie, Y.P. Gao, T.C. An, Appl. Catal. B 180 (2016) 726–732.
[7] H.M. Bai, P. He, J. Pan, J.C. Chen, Y. Chen, F.Q. Dong, H. Li, J. Colloid Interface Sci. 497 (2017) 422–428.
[8] G.M. Liu, X.Z. Li, J.C. Zhao, H. Hidaka, N. Serpone, Environ. Sci. Technol. 34 (2000) 3982–3990.
[9] C.C. Wang, J.R. Li, X.L. Lv, Y.Q. Zhang, G.S. Guo, Energy Environ. Sci. 7 (2014) 2831–2867.
[10] P. Zhou, J.G. Yu, M. Jaroniec, Adv. Mater. 26 (2014) 4920–4935.
[11] Y.Z. Hong, Y.H. Jiang, C.S. Li, W.Q. Fan, X. Yan, M. Yan, W.D. Shi, Appl. Catal. B 180 (2016) 663–673.
[12] J.J. Jiang, H.T. Wang, X.D. Chen, S. Li, T.F. Xie, D.J. Wang, Y.H. Lin, J. Colloids Interface Sci. 494 (2017) 130–138.
[13] X.H. Sun, Q. Zhang, H. Liang, L. Ying, X.X. Meng, V.K. Sharma, J. Hazard. Mater. 319 (2016) 130–136.
[14] D.G. Li, X.G. Duan, H.Q. Sun, J. Kang, H.Y. Zhang, M.O. Tade, S.B. Wang, Carbon 115 (2017) 649–658.
[15] Z.S. Liang, G.Y. Li, T.C. An, Environ. Pollut. 225 (2017) 104–111.
[16] J.L. Yu, E. Philip, Appl. Catal. B 31 (2001) 123–132.
[17] A. Jain, S. Jayaraman, G. Singh, M.P. Srinivasan, J. Supercrit. Fluids 116 (2016) 209–214.
[18] P. Niu, L.C. Yin, Y.Q. Yang, G. Liu, H.M. Cheng, Adv. Mater. 26 (2014) 8046–8052.
[19] M. Wu, J.M. Yan, X.N. Tang, M. Zhao, Q. Jiang, ChemSusChem 7 (2014) 2654–2658.
[20] H.Q. Sun, G.L. Zhou, Y.X. Wang, A. Suvorova, S.B. Wang, ACS Appl. Mater. Interface 6 (2014) 16745–16754.
[21] S.C. Yan, Z.S. Li, Z.G. Zou, Langmuir 25 (2009) 10397–10401.
[22] J.S. Zhang, Y. Chen, X.C. Wang, Energy Environ. Sci. 8 (2015) 3092–3108.
[23] Y. Zhang, L.H. Lin, B. Wang, X.C. Wang, Angew. Chem. Int. Ed. 54 (2015) 12868–12884.
[24] G.G. Zhang, Z.A. Lan, L.H. Lin, S. Lin, X.C. Wang, Chem. Sci. 7 (2016) 3062–3066.
[25] X.C. Wang, S. Blechert, M. Antonietti, ACS Catal. 2 (2012) 1596–1606.
[26] L. Ge, C.C. Han, J. Liu, Y.F. Li, Appl. Catal. A 409 (2011) 215–222.
[27] X.J. Bai, R.L. Zong, C.X. Li, D. Liu, Y.F. Liu, Y.F. Zhu, Appl. Catal. B 147 (2014) 82–91.
[28] Y.Y. Bu, Z.Y. Chen, W.B. Li, Appl. Catal. B 144 (2014) 622–630.
[29] M. Xu, L. Han, S. Dong, ACS Appl. Mater. Interface 5 (2013) 12533–12540.
[30] M. Wu, J.M. Yan, X.W. Zhang, M. Zhao, Q. Jiang, J. Mater. Chem. A 3 (2015) 15710–15714.
[31] L. Shi, L. Liang, J. Ma, F.X. Wang, J.M. Sun, Catal. Sci. Technol. 4 (2014) 758–765.
[32] H.T. Ren, S.Y. Jia, Y. Wu, S.H. Wu, T.H. Zhang, X. Han, Ind. Eng. Chem. Res. 53 (2014) 17654–17663.
[33] N. Tian, H. Huang, Y. He, Y. Guo, Y. Zhang, Colloids Surf. A 467 (2015) 188–194.
[34] J. Wang, P. Guo, M.F. Dou, J. Wang, Y.J. Cheng, P. Jonsson, Z. Zhao, RSC Adv. 4 (2014) 51008–51015.
[35] H.F. Shi, C.L. Zhang, C.P. Zhou, RSC Adv. 5 (2015) 50146–50154.
[36] S. Kumar, T. Surendar, A. Baruah, V. Shanker, J. Mater. Chem. A 1 (2013) 5333–5340.
[37] Y.M. He, L.H. Zhang, B.T. Teng, M.H. Fan, Environ. Sci. Technol. 49 (2015) 649–656.
[38] K. Dai, J.L. Lv, L.H. Lu, C.H. Liang, L. Geng, G.P. Zhu, Mater. Chem. Phys. 177 (2016) 529–537.
[39] D.M. Chen, Z.H. Wang, Y. Du, G.L. Yang, T.Z. Ren, H. Ding, Catal. Today 258 (2015)

41–48.
[40] A. Akhundi, A. Habibi-Yangjeh, J. Colloid Interface Sci. 482 (2016) 165–174.
[41] H. Xu, J. Yan, Y.G. Xu, Y.H. Song, H.M. Li, J.X. Xia, C.J. Huang, H.L. Wan, Appl. Catal. B 180 (2016) 530–543.
[42] Y. Bao, K. Chen, Nano-Micro Lett. 8 (2015) 182–192.
[43] Y.Y. Shang, X. Chen, W.W. Liu, P.F. Tan, H.Y. Chen, L.D. Wu, C. Ma, X. Xiong, J. Pan, Appl. Catal. B 204 (2017) 78–88.
[44] J.V. Kumar, R. Karthik, S.M. Chen, V. Muthuraj, C. Karuppiah, Sci. Rep. (2016) 34149.
[45] M.T. Fabbro, C.C. Foggi, L.P.S. Santos, L. Gracia, A. Perrin, C. Perrin, C.E. Vergani, A.L. Machado, J. Andres, E. Cordoncillo, E. Longo, Dalton Trans. 45 (2016) 10736–10743.
[46] J.V.B. Moura, J.G.D.S. Filho, P.T.C. Freire, C. Luz-Lima, G.S. Pinheiro, B.C. Viana, J.M. Filho, A.G. Souza-Filho, G.D. Saraiva, Vib. Spectrosc. 86 (2016) 97–102.
[47] Y.Y. Bai, Y. Lu, J.K. Liu, J. Hazard. Mater. 307 (2016) 26–35.
[48] Y.Y. Bai, F.R. Wang, J.K. Liu, Ind. Eng. Chem. Res. 55 (2016) 9873–9879.
[49] J.Y. Zhang, Y. Lu, J.K. Liu, H. Jiang, RSC. Adv. 6 (2016) 9477.
[50] J. Andres, M.M. Ferrer, L. Gracia, A. Beltran, V.M. Longo, G.H. Cruvinel, R.L. Tranquilin, E. Longo, Part. Part. Syst. Charact. 32 (2015) 646–651.
[51] D.F. Xu, B. Cheng, J.F. Zhang, W.K. Wang, J.G. Yu, W.K. Ho, J. Mater. Chem. A 3 (2015) 20153–20166.
[52] J.L. Zhang, Z. Ma, RSC Adv. 7 (2017) 2163–2171.
[53] Y.W. Zhang, J.H. Liu, G. Wu, W. Chen, Nanoscle 4 (2012) 5300–5303.
[54] J.D. Hong, X.Y. Xia, Y.S. Wang, R. Xu, J. Mater. Chem. 22 (2012) 15006–15012.
[55] J.H. Liu, T.K. Zhang, Z.C. Wang, G. Dawson, W. Chen, J. Mater. Chem. 22 (2012) 15006–15012.
[56] J.S. Zhang, M.W. Zhang, G.G. Zhang, X.C. Wang, ACS Catal. 26 (2012) 940–948.
[57] L. Ge, C.C. Han, Appl. Catal. B 117–118 (2012) 268–274.
[58] Z.Z. Lin, X.C. Wang, Angew. Chem. Int. Ed. 52 (2013) 1735–1738.
[59] J.H. Li, B.A. Shen, Z.H. Hong, B.Z. Lin, B.F. Gao, Y.L. Chen, Chem. Commun. 48 (2012) 12017–12019.
[60] X.W. Wang, G. Liu, Z.G. Chen, F. Li, L.Z. Wang, G.Q. Lu, H.M. Cheng, Chem. Commun. 23 (2009) 3452–3454.
[61] G.Q. Tan, L.N. She, T. Liu, C. Xu, H.J. Ren, A. Xia, Appl. Catal. B 207 (2017) 120–133.
[62] H.H. Ji, F. Chang, X.F. Hu, W. Qin, J.W. Shen, Chem. Eng. J. 218 (2013) 183–190.
[63] R. Dhanabal, S. Velmathi, A.C. Bose, Catal. Sci. Technol. 6 (2016) 8449–8484.